Universität Karlsruhe (TH)
Institut für Baustatik

Elastic and plastic analysis of thin–walled structures using improved hexahedral elements

W. Wagner, S. Klinkel, F. Gruttmann

Mitteilung 3(2001)

Universität Karlsruhe (TH)
Institut für Baustatik

Elastic and plastic analysis of thin–walled structures using improved hexahedral elements

W. Wagner, S. Klinkel, F. Gruttmann

Mitteilung 3(2001)

Prof. Dr.–Ing. W. Wagner
Institut für Baustatik
Universität Karlsruhe
Postfach 6980
76128 Karlsruhe

Telefon: (0721) 608–2280
Telefax: (0721) 608–6015
E–mail: bs@.uni-karlsruhe.de
Internet: http://www.bs.uni-karlsruhe.de

Elastic and plastic analysis of thin–walled structures using improved hexahedral elements

W. Wagner [a] *, S. Klinkel [a], F. Gruttmann [b]

[a] Institut für Baustatik, Universität Karlsruhe (TH), Kaiserstraße 12, D-76131 Karlsruhe, Germany

[b] Institut für Statik, Technische Universität Darmstadt, Alexanderstraße 7, D-64283 Darmstadt, Germany

Abstract

In this paper a continuum based 3D–shell element for the nonlinear analysis of thin-walled structures is developed. Assumed natural strain method and enhanced assumed strain method are used to improve the relative poor element behaviour of a standard hexahedral displacement element. Different elastic and inelastic constitutive laws are considered. The anisotropic material behaviour of layered shells is modeled using a hyperelastic orthotropic material law in each layer. Furthermore, finite multiplicative J_2-plasticity is discussed. The models are characterized by an interface to the material setting of the boundary value problem. Several examples show the applicability and efficiency of the developed element formulation.

Keywords: Shell element, three–dimensional constitutive equations, linear elastic orthotropic material law, finite strain plasticity

1 Introduction

The efficient computation of thin structures in structural mechanics requires reliable and robust elements. Several shell elements have been developed in the past, where the normal stresses in thickness direction have been incorporated in the variational formulation. The kinematic degrees of freedom are the components of the displacement vector and of the extensible director vector of the reference surface, see e.g [1–4], among many others. The stresses are evaluated from a three–dimensional material law. This feature is especially useful for complicated nonlinear constitutive equations. Locking effects, which occur if a three–dimensional material law is used along with constant normal thickness strains, can be avoided. This has been done in [2] applying the enhanced assumed strain method to the thickness strains. The associated variational formulation of this method has been developed in [5,6].

For certain problems in structural analysis nodal degrees of freedom at the surface of the shell are more advantageous. Examples are deformation processes with contact and friction or the delamination problem of layered shells. For this purpose surface oriented shell elements have been developed e. g. in [7–10].

In this paper we describe a continuum based shell element and application to some geometrical and physical nonlinear problems. The essential features of the present formulation are summarized as follows.

* Corresponding author. Present Address: Institut für Baustatik, Universität Karlsruhe (TH), Kaiserstraße 12, D-76131 Karlsruhe, Germany. Tel: +49-721-608-2280; Fax: +49-721-608-6015. *E-mail*: bs@uni-karlsruhe.de.

(i) The shell is parameterized using convective coordinates. Thus, the components of the stress and strain tensors refer to local convective base vectors. The basic hexahedral element using tri–linear shape functions possesses three displacement degrees of freedom at the nodes. Boundary conditions at the top or bottom surface of the shell can be considered.

(ii) The relative poor behaviour of the standard displacement element is improved using the assumed strain method and the enhanced strain method. To avoid shear locking the assumed natural strain method is applied to the transverse shear strains, see [11] for plates. Furthermore the thickness strains are approximated using special interpolation functions introduced in [3] for a shell formulation with an extensible director vector. This is necessary to avoid artificial thickness strains. The membrane behaviour and the bending behaviour is essentially improved applying the enhanced assumed strain method to the membrane strains and to the thickness strains. The associated variational formulation is written in a Lagrangian setting using the Green–Lagrangian strain tensor. Due to the different approximations of the strain components the element possesses an orientation which has to be considered within the mesh generation.

(iii) Different three–dimensional constitutive laws are implemented. For laminated structures with privileged directions a hyperelastic anisotropic material law is given. The strain energy is formulated using so–called structural tensors. One obtains a coordinate invariant formulation and material frame indifference is automatically fulfilled. Furthermore we consider finite J_2-plasticity along with isotropic elastic behaviour. Here we present a material formulation of the theory, see also [12] for membranes. In this case the interface to the assumed strain formulation using Lagrangian strain measures is preserved.

2 Basic equations

Let X be a material point of the considered structure B and denote by $\mathbf{X}$ and $\mathbf{x}$ the position vectors of X in the reference and current configurations, respectively. The motion $\boldsymbol{\chi}$ is a mapping, such that $\mathbf{x} = \boldsymbol{\chi}(\mathbf{X}, t)$ at time t. Hence, recall that the deformation gradient $\mathbf{F}$ at a material point is defined as $\mathbf{F} := \partial\boldsymbol{\chi}/\partial\mathbf{X}$. The displacement field $\mathbf{u}$ is obtained with $\mathbf{u}(\mathbf{X}, t) = \boldsymbol{\chi}(\mathbf{X}, t) - \mathbf{X}$. With the assumptions that the function $\boldsymbol{\chi}$ is sufficiently smooth and $\det \mathbf{F} = 1$ at $t = 0$, invertibility of the motion requires that $J = \det \mathbf{F} > 0$ for all $(\mathbf{X}, t)$. Furthermore we denote by ρ_0 and $\rho = J\,\rho_0$ the density at a material point in the reference and current configuration, respectively. In a standard way the right Cauchy–Green tensor is introduced as $\mathbf{C} := \mathbf{F}^T\mathbf{F}$ and the Green–Lagrangian strain tensor as $\mathbf{E} := \frac{1}{2}(\mathbf{C} - \mathbf{1})$ with the second order unit tensor $\mathbf{1}$.

The considered shell is parameterized by convective coordinates, where ξ^1 and ξ^2 are inplane coordinates and ξ^3 denotes the thickness coordinate. Hence the covariant base vectors are obtained by partial derivatives of the position vectors with respect to the convective coordinates ξ^i , $i = 1, 2, 3$

$$\mathbf{G}_i = \frac{\partial \mathbf{X}}{\partial \xi^i} \,, \qquad \mathbf{g}_i = \frac{\partial \mathbf{x}}{\partial \xi^i} \,, \tag{1}$$

whereas the contravariant base vectors are defined by $\mathbf{G}_i \cdot \mathbf{G}^j = \delta_i^j$ and $\mathbf{g}_i \cdot \mathbf{g}^j = \delta_i^j$. The deformation gradient can be written as $\mathbf{F} = \mathbf{g}_i \otimes \mathbf{G}^i$. This leads to the following representation of the Green–Lagrangian strain tensor

$$\mathbf{E} = E_{ij}\ \mathbf{G}^i \otimes \mathbf{G}^j \,, \qquad E_{ij} = \frac{1}{2}\ (g_{ij} - G_{ij}) \,, \tag{2}$$

where $g_{ij} = \mathbf{g}_i \cdot \mathbf{g}_j$ and $G_{ij} = \mathbf{G}_i \cdot \mathbf{G}_j$ denote the metric coefficients of the current configuration and of the reference configuration, respectively.

We assume surface loading $\hat{\mathbf{t}}$ and volume forces $\rho_0 \hat{\mathbf{b}}$ acting on the shell. Following the approach in [13] and [14] the three-field variational functional is given in a material formulation

$$\Pi(\mathbf{u}, \tilde{\mathbf{E}}, \tilde{\mathbf{S}}) = \int_{B_0} (\psi(\mathbf{E} + \tilde{\mathbf{E}}) - \tilde{\mathbf{S}} : \tilde{\mathbf{E}}) \, \mathrm{d}V - \int_{B_0} \rho_0 \hat{\mathbf{b}} \cdot \mathbf{u} \, \mathrm{d}V - \int_{\partial B_0} \hat{\mathbf{t}} \cdot \mathbf{u} \, \mathrm{d}A \,, \tag{3}$$

where ψ denotes the elastic free energy per unit volume of the reference configuration. Note, that Π is a function of the independent tensorial quantities $\mathbf{u}$, $\tilde{\mathbf{E}}$ and $\tilde{\mathbf{S}}$, where $\tilde{\mathbf{E}}$ denotes the so–called enhanced strain tensor and $\tilde{\mathbf{S}}$ the independent stress tensor. Introducing an orthogonality condition for the stress field $\tilde{\mathbf{S}}$ and the enhanced strain field $\tilde{\mathbf{E}}$ the variational formulation can be reduced to a two–field problem. The first and second variation of above functional are specified in detail in Klinkel et al. [10].

In the following we discuss the essential features of the finite element formulation. First, the position vectors of the reference and current configuration are approximated as follows

$$\mathbf{X}^h = \sum_{I=1}^{nel} N_I(\xi^1, \xi^2, \xi^3) \mathbf{X}_I \qquad\qquad \mathbf{x}^h = \sum_{I=1}^{nel} N_I(\xi^1, \xi^2, \xi^3) \mathbf{x}_I \,, \tag{4}$$

with $nel = 8$ and $N_I(\xi^1, \xi^2, \xi^3) = \frac{1}{8}(1 + \xi_I^1 \xi^1)(1 + \xi_I^2 \xi^2)(1 + \xi_I^3 \xi^3)$. The index h is used to denote the finite element approximation.

It is well–known that above displacement formulation is too stiff, especially when these elements are used to discretize thin structures. Therefore we apply the assumed strain method to reduce the locking effects. To avoid shear locking the transverse shear strains are approximated using the interpolation functions of Bathe and Dvorkin [11]. For thin shell structures with bending dominated loading locking due to artificial thickness strains has been observed by Ramm et al. in [15] when using a direct interpolation of the director vector. To improve the element behaviour an ANS–interpolation of the thickness strains E_{33} using bi–linear shape functions for four–node shell elements have been proposed e.g. by Betsch, Stein in [3]. Here, we adapt this procedure to the hexahedral element, see [10]. Numerical investigations showed that it is sufficient to apply the approximations in the middle plane of the element.

The membrane behaviour of the element can be essentially improved using the enhanced assumed strain method. The components of the enhanced strain tensor as are introduced in (3) are given with respect to different base vectors

$$\tilde{\mathbf{E}} = \tilde{E}_{ij} \, \mathbf{G}^i \otimes \mathbf{G}^j = \frac{\det \mathbf{J}_0}{\det \mathbf{J}} \, \tilde{E}_{ij}^0 \, \mathbf{G}_0^i \otimes \mathbf{G}_0^j \,, \tag{5}$$

with $\mathbf{J} = [\mathbf{G}_1, \ \mathbf{G}_2, \ \mathbf{G}_3]$. The vectors $\mathbf{G}_0^i$ and matrix $\mathbf{J}_0$ are evaluated at the element center. Following common usage in the finite element literature we arrange the tensor components in a vector as follows

$$\mathbf{E} = [E_{11}, E_{22}, E_{33}, 2\,E_{12}, 2\,E_{13}, 2\,E_{23}]^T \,. \tag{6}$$

From (5) we obtain the matrix representation

$$\tilde{\mathbf{E}} = \frac{\det \mathbf{J}_0}{\det \mathbf{J}} \, \mathbf{T}_E^0 \, \tilde{\mathbf{E}}^0 \qquad \text{with} \qquad \tilde{\mathbf{E}}^0 = \mathbf{M}(\xi^1, \xi^2, \xi^3) \, \boldsymbol{\alpha}^e \,. \tag{7}$$

Here, $\mathbf{T}_E^0$ denotes a transformation matrix and $\mathbf{M}$ the interpolation matrix associated with 5 or 8 independent parameters arranged in the vector $\boldsymbol{\alpha}^e$. All matrices are specified in detail in Klinkel et al. [10].

Remark:
An alternative enhanced strain formulation for extensible shells is given in Betsch [16]. Following Simo and Rifai [6] the material deformation gradient is enhanced in [16] with incompatible parts for the membrane and thickness strains. Numerical investigations showed no significant differences to the enhanced strain formulation using the Green–Lagrangian strain tensor even in the range of finite strains. The advantage of the latter formulation lies in the fact that the geometric stiffness matrix corresponds to the one of the displacement formulation.

3 Orthotropic elastic material

In this section we formulate the constitutive equations for layered fiber reinforced composite shells. Assuming orthotropic elastic material behaviour the privileged directions are described by the orthogonal base system $\mathbf{t}^i\,, i = 1, 2, 3$. The tensor products

$$ {}^1\mathbf{M} = \mathbf{t}^1 \otimes \mathbf{t}^1 \qquad {}^2\mathbf{M} = \mathbf{t}^2 \otimes \mathbf{t}^2 \qquad {}^3\mathbf{M} = \mathbf{t}^3 \otimes \mathbf{t}^3 \tag{8} $$

are called structural tensors. The third tensor ${}^3\mathbf{M}$ is not independent and can be replaced using ${}^1\mathbf{M} + {}^2\mathbf{M} + {}^3\mathbf{M} = \mathbf{1}$.

According to [17], [18] the elastic free energy can be written as a function of the structural tensors and the linear strain tensor $\boldsymbol{\varepsilon}$ as $\psi = \psi(\boldsymbol{\varepsilon},\, {}^1\mathbf{M},\, {}^2\mathbf{M})$. Here, for the geometrical nonlinear range with moderately large strains the strain energy is assumed to be a quadratic function of the invariants

$$ \operatorname{tr}\mathbf{E}\,,\ \operatorname{tr}\mathbf{E}^2\,,\ \operatorname{tr}({}^1\mathbf{M}\mathbf{E})\,,\ \operatorname{tr}({}^1\mathbf{M}\mathbf{E}^2)\,,\ \operatorname{tr}({}^2\mathbf{M}\mathbf{E})\,,\ \operatorname{tr}({}^2\mathbf{M}\mathbf{E}^2)\,. \tag{9} $$

With the assumption of a stress free reference configuration ψ is given as

$$ \begin{aligned} \psi(\mathbf{E},\, {}^1\mathbf{M},\, {}^2\mathbf{M})) = & \frac{\lambda}{2}\,(\operatorname{tr}\mathbf{E})^2 + \mu\ \operatorname{tr}\mathbf{E}^2 \\ & + (\alpha_1\ \operatorname{tr}({}^1\mathbf{M}\mathbf{E}) + \alpha_2\ \operatorname{tr}({}^2\mathbf{M}\mathbf{E}))\ \operatorname{tr}\mathbf{E} \\ & + 2\mu_1\ \operatorname{tr}({}^1\mathbf{M}\mathbf{E}^2) + 2\mu_2\ \operatorname{tr}({}^2\mathbf{M}\mathbf{E}^2) \\ & + \frac{\beta_1}{2}(\operatorname{tr}({}^1\mathbf{M}\mathbf{E}))^2 + \frac{\beta_2}{2}(\operatorname{tr}({}^2\mathbf{M}\mathbf{E}))^2 \\ & + \beta_3(\operatorname{tr}({}^1\mathbf{M}\mathbf{E}))(\operatorname{tr}({}^2\mathbf{M}\mathbf{E}))\,. \end{aligned} \tag{10} $$

The nine parameters λ, μ, μ_1, μ_2, α_1, α_2, β_1, β_2, β_3 are independent material constants. The relation to the classical engineering parameters E_1, E_2, E_3, ν_{12}, ν_{13}, ν_{23} and G_{12}, G_{13}, G_{23} can be derived, see e.g. [18]. Transversal isotropic behaviour is included as special case. This function leads to a coordinate invariant representation of an orthotropic constitutive law.

The derivative of (10) with respect to the Green–Lagrangian strain tensor yields the work

conjugate Second Piola–Kirchhoff stress tensor

$$\begin{aligned}\mathbf{S} = \frac{\partial \psi}{\partial \mathbf{E}} &= \lambda\ \mathrm{tr}\,\mathbf{E}\,\mathbf{1} + 2\mu\,\mathbf{E} \\ &+(\alpha_1\,\mathbf{t}^1\cdot\mathbf{E}\mathbf{t}^1 + \alpha_2\,\mathbf{t}^2\cdot\mathbf{E}\mathbf{t}^2)\,\mathbf{1} \\ &+(\alpha_1\,\mathbf{t}^1\otimes\mathbf{t}^1 + \alpha_2\,\mathbf{t}^2\otimes\mathbf{t}^2)\ \mathrm{tr}\,\mathbf{E} \\ &+2\mu_1\,(\mathbf{t}^1\otimes\mathbf{t}^1\mathbf{E} + \mathbf{E}\mathbf{t}^1\otimes\mathbf{t}^1) \\ &+2\mu_2\,(\mathbf{t}^2\otimes\mathbf{t}^2\mathbf{E} + \mathbf{E}\mathbf{t}^2\otimes\mathbf{t}^2)) \\ &+\beta_1(\mathbf{t}^1\cdot\mathbf{E}\mathbf{t}^1)\mathbf{t}^1\otimes\mathbf{t}^1 + \beta_2(\mathbf{t}^2\cdot\mathbf{E}\mathbf{t}^2)\mathbf{t}^2\otimes\mathbf{t}^2 \\ &+\beta_3(\mathbf{t}^1\cdot\mathbf{E}\mathbf{t}^1)\mathbf{t}^2\otimes\mathbf{t}^2 + (\mathbf{t}^2\cdot\mathbf{E}\mathbf{t}^2)\mathbf{t}^1\otimes\mathbf{t}^1)\quad .\end{aligned} \tag{11}$$

The second derivative yields the symmetric and constant material tensor

$$\begin{aligned}\mathbb{C} = \frac{\partial^2 \psi}{\partial \mathbf{E}^2} &= \lambda\,\mathbf{1}\otimes\mathbf{1} + 2\mu\,\mathbb{I} \\ &+\alpha_1\,[(\mathbf{t}^1\otimes\mathbf{t}^1)\otimes\mathbf{1} + \mathbf{1}\otimes(\mathbf{t}^1\otimes\mathbf{t}^1)] \\ &+\alpha_2\,[(\mathbf{t}^2\otimes\mathbf{t}^2)\otimes\mathbf{1} + \mathbf{1}\otimes(\mathbf{t}^2\otimes\mathbf{t}^2)] \\ &+2\mu_1\,(\mathbf{t}^1\otimes\mathbb{I}^{[2]}\mathbf{t}^1 + \mathbf{t}^{1\,[2]}\mathbb{I}\otimes\mathbf{t}^1) \\ &+2\mu_2\,(\mathbf{t}^2\otimes\mathbb{I}^{[2]}\mathbf{t}^2 + \mathbf{t}^{2\,[2]}\mathbb{I}\otimes\mathbf{t}^2) \\ &+\beta_1\,(\mathbf{t}^1\otimes\mathbf{t}^1\otimes\mathbf{t}^1\otimes\mathbf{t}^1) + \beta_2\,(\mathbf{t}^2\otimes\mathbf{t}^2\otimes\mathbf{t}^2\otimes\mathbf{t}^2) \\ &+\beta_3\,(\mathbf{t}^1\otimes\mathbf{t}^1\otimes\mathbf{t}^2\otimes\mathbf{t}^2 + \mathbf{t}^2\otimes\mathbf{t}^2\otimes\mathbf{t}^1\otimes\mathbf{t}^1)\end{aligned} \tag{12}$$

with

$$\begin{aligned}\mathbf{t}^1\otimes\mathbb{I}^{[2]}\mathbf{t}^1 &= t^{1\,i}\,G^{jk}\,t^{1\,l}\,(\mathbf{G}_i\otimes\mathbf{G}_j\otimes\mathbf{G}_k\otimes\mathbf{G}_l) \\ \mathbf{t}^{2\,[2]}\mathbb{I}\otimes\mathbf{t}^2 &= G^{ij}\,t^{2\,k}\,t^{2\,l}\,(\mathbf{G}_i\otimes\mathbf{G}_j\otimes\mathbf{G}_k\otimes\mathbf{G}_l)\end{aligned} \tag{13}$$

and

$$\begin{aligned}\mathbf{1} &= G^{ij}\,\mathbf{G}_i\otimes\mathbf{G}_j \\ \mathbb{I} &= G^{ik}G^{jl}\,(\mathbf{G}_i\otimes\mathbf{G}_j\otimes\mathbf{G}_k\otimes\mathbf{G}_l)\quad .\end{aligned} \tag{14}$$

The components of $\mathbf{t}^1$, $\mathbf{t}^2$ are given with respect to the convective base vectors $\mathbf{G}_i$.

4 Finite J_2-plasticity

In this section a framework of finite J_2-plasticity in a material setting is presented. As basic kinematic assumption we introduce the multiplicative decomposition of the deformation gradient in elastic and plastic part $\mathbf{F} = \mathbf{F}^e\,\mathbf{F}^p$. This implies a stress free intermediate configuration which is defined by $\mathbf{F}^{e-1}$. It is well–known that the decomposition is unique up to a rotation. The relevant strain tensors are defined as follows

$$\begin{aligned}\mathbf{C} &= \mathbf{F}^T\,\mathbf{F} & \mathbf{b} &= \mathbf{F}\,\mathbf{F}^T \\ \mathbf{C}^p &= \mathbf{F}^{pT}\,\mathbf{F}^p & \mathbf{b}^p &= \mathbf{F}^p\,\mathbf{F}^{pT} \\ \mathbf{C}^e &= \mathbf{F}^{eT}\,\mathbf{F}^e & \mathbf{b}^e &= \mathbf{F}^e\,\mathbf{F}^{eT}\,.\end{aligned} \tag{15}$$

The constitutive equations are restricted by the dissipation inequality. The local dissipation function D per unit of the reference volume is defined as the difference between the local stress power and the local rate of the free energy $D = \boldsymbol{\tau} : \mathbf{d} - \dot{\psi} \geq 0$. Here, $\mathbf{d} = \mathbf{F}^{-T}\dot{\mathbf{E}}\mathbf{F}^{-1}$ denotes the rate of deformation tensor and $\boldsymbol{\tau} = \mathbf{F}\mathbf{S}\mathbf{F}^T$ is the Kirchhoff stress tensor. Introducing the free energy $\psi = \psi(\mathbf{b}_e, \bar{\varepsilon})$ as function of the elastic left Cauchy–Green tensor $\mathbf{b}^e$ and the internal variable $\bar{\varepsilon}$, the time derivative of ψ can be expressed with $\mathbf{b}^e = \mathbf{F}\mathbf{C}^{p-1}\mathbf{F}^T$. Following standard arguments in thermodynamics with internal state variables, one obtains the constitutive equation

$$\boldsymbol{\tau} = 2\,\frac{\partial \psi}{\partial \mathbf{b}^e}\,\mathbf{b}^e\,. \tag{16}$$

Hence, considering $\dot{\mathbf{C}}^{p-1}\,\mathbf{C}^p = -\mathbf{C}^{p-1}\,\dot{\mathbf{C}}^p$ the reduced dissipation inequality reads
$D = \boldsymbol{\tau} \,:\, \frac{1}{2}\,\mathbf{F}\mathbf{C}^{p-1}\dot{\mathbf{C}}^p\mathbf{F}^{-1} + \zeta\,\dot{\bar{\varepsilon}} \geq 0$, where $\zeta := -\partial\psi/\partial\bar{\varepsilon}$ is thermodynamic conjugate to $\bar{\varepsilon}$.

The evolution equations for the plastic strains are derived using the principle of maximum plastic dissipation. Thus, the actual state $(\boldsymbol{\tau}, \zeta)$ leads to maximum dissipation among all admissible states $(\tilde{\boldsymbol{\tau}}, \tilde{\zeta}) \in E$:

$$(\tilde{\boldsymbol{\tau}} - \boldsymbol{\tau}) \,:\, \frac{1}{2}\,\mathbf{F}\mathbf{C}^{p-1}\dot{\mathbf{C}}^p\mathbf{F}^{-1} + (\tilde{\zeta} - \zeta)\,\dot{\bar{\varepsilon}} \leq 0\,. \tag{17}$$

If E, defined by the yield condition $\phi(\boldsymbol{\tau}, \zeta) \leq 0$, is a convex domain, a standard result in convex analysis yields along with the loading–unloading condition $\dot{\gamma} \geq 0, \phi \leq 0, \dot{\gamma}\phi = 0$ the normality rule for the inelastic strains

$$\begin{aligned} \frac{1}{2}\,\mathbf{F}\mathbf{C}^{p-1}\dot{\mathbf{C}}^p\mathbf{F}^{-1} &= \dot{\gamma}\,\frac{\partial \phi}{\partial \boldsymbol{\tau}} \\ \dot{\bar{\varepsilon}} &= \dot{\gamma}\,\frac{\partial \phi}{\partial \zeta} \end{aligned} \tag{18}$$

Thus we obtain the flow rule in a Lagrangian setting. The corresponding spatial representation is given in [19] or [20].

The flow rule is approximately integrated using the so–called exponential mapping, e.g. [21]. With this type of integration the condition of plastic incompressibility is exactly preserved, see e.g. [20]. The rate of the equivalent plastic strain is integrated using the standard backward Euler integration algorithm. Within a time interval $[t_n, t_{n+1}]$ one obtains

$$\begin{aligned} \mathbf{C}^p_{n+1} &= \mathbf{C}^p_n\,\exp[2\,\gamma_{n+1}\,(\mathbf{F}^{-1}_{n+1}\,\frac{\partial \phi_{n+1}}{\partial \boldsymbol{\tau}_{n+1}}\,\mathbf{F}_{n+1})] \\ \bar{\varepsilon}_{n+1} &= \bar{\varepsilon}_n + \gamma_{n+1}\frac{\partial \phi_{n+1}}{\partial \zeta_{n+1}}\,, \end{aligned} \tag{19}$$

where $\gamma_{n+1} := (t_{n+1} - t_n)\,\dot{\gamma}_{n+1}$ is the so–called consistency parameter.

To evaluate the exponential function we introduce the spectral decomposition of the relevant strain tensors. First, the spectral decompositions of the deformation gradient and its inverse are given

$$\mathbf{F} = \sum_{A=1}^{3} \lambda^e_A\,\mathbf{n}_A \otimes \hat{\mathbf{N}}_A \qquad , \qquad \mathbf{F}^{-1} = \sum_{A=1}^{3} \frac{1}{\lambda^e_A}\,\hat{\mathbf{N}}^A \otimes \mathbf{n}_A\,, \tag{20}$$

with the elastic stretches λ^e_A and the below defined eigenvectors.

The elastic principal stretches can be evaluated solving the eigenvalue problem with respect to the three different configurations, see e.g. [22]. Here, we use a Lagrangian representation

$$(\mathbf{C} - \lambda^{e\,2}_A\mathbf{C}^p)\,\hat{\mathbf{N}}^A = \mathbf{0} \quad \text{with} \quad \hat{\mathbf{N}}^A \cdot \mathbf{C}^p\,\hat{\mathbf{N}}^B = \delta^{AB}\,, \tag{21}$$

where $\mathbf{C}^p = \sum_{A=1}^{3} \hat{\mathbf{N}}_A \otimes \hat{\mathbf{N}}_A$. With this approach the interface to the above documented finite element formulation is automatically maintained.

Eq. (21) implies an eigenvector basis, which is defined by

$$\hat{\mathbf{N}}^A \cdot \hat{\mathbf{N}}_B = \delta^A_B \qquad , \qquad \hat{\mathbf{N}}^A = \frac{1}{\lambda^p_A}\,\mathbf{N}^A \qquad , \qquad \hat{\mathbf{N}}_B = \lambda^p_B\,\mathbf{N}^B\,. \tag{22}$$

Introducing the spectral decomposition $\mathbf{F}^{-1}\,\frac{\partial \phi}{\partial \boldsymbol{\tau}}\,\mathbf{F} = \sum_{A=1}^{3} \frac{\partial \phi}{\partial \tau_A}\,\hat{\mathbf{N}}^A \otimes \hat{\mathbf{N}}_A$ eq. $(19)_1$ is rewritten as

$$\mathbf{C}^p_{trial} := \mathbf{C}^p_n = \sum_{A=1}^{3} \exp[-2\gamma_{n+1}\frac{\partial \phi_{n+1}}{\partial \tau_{A_{n+1}}}]\,\hat{\mathbf{N}}_{A_{n+1}} \otimes \hat{\mathbf{N}}_{A_{n+1}} \tag{23}$$

and with $\mathbf{C}^p_{trial} = \sum_{A=1}^{3} \hat{\mathbf{N}}_{A_{trial}} \otimes \hat{\mathbf{N}}_{A_{trial}}$ we define

$$\begin{aligned} \hat{\mathbf{N}}_{A_{trial}} &:= \tfrac{\lambda^e_{A_{n+1}}}{\lambda^e_{A_{trial}}}\hat{\mathbf{N}}_{A_{n+1}} \\ \lambda^{e\,2}_{A_{trial}} &:= \exp[2\gamma_{n+1}\,\frac{\partial \phi_{n+1}}{\partial \tau_{A_{n+1}}}]\lambda^{e\,2}_{A_{n+1}}\,. \end{aligned} \tag{24}$$

Thus, the elastic trial stretches are computed with the solution of the general eigenvalue problem

$$(\mathbf{C} - \lambda^{e\,2}_{A_{trial}}\mathbf{C}^p_{trial})\,\hat{\mathbf{N}}^A{}_{trial} = \mathbf{0}\,. \tag{25}$$

To complete the formulation we now specify the free energy $\psi(\mathbf{b}_e, \bar{\varepsilon}) = \psi_{el}(\mathbf{b}_e) + \psi_{pl}(\bar{\varepsilon})$ in a decoupled form, where $\psi_{pl}(\bar{\varepsilon})$ denotes the part due to isotropic plastic hardening. The internal variable $\bar{\varepsilon}$ corresponds to the equivalent plastic strain. For isotropic material behaviour the strain energy $\psi_{el}(\mathbf{b}_e)$ can be expressed in terms of the eigenvalues of $\mathbf{b}_e$. Here, the elastic strain energy is postulated as a quadratic function of the logarithmic strains $\varepsilon_A = \log(\lambda^e_A)$

$$\psi_{el} = \frac{\lambda}{2}[\varepsilon^e_1 + \varepsilon^e_2 + \varepsilon^e_3]^2 + \mu[(\varepsilon^e_1)^2 + (\varepsilon^e_2)^2 + (\varepsilon^e_3)^2] \tag{26}$$

with the Lamé parameters λ and μ. Introducing the vectors $\boldsymbol{\varepsilon}^e = (\varepsilon^e_1,\, \varepsilon^e_2,\, \varepsilon^e_3)^T$ and $\tilde{\boldsymbol{\tau}} = (\tau_1,\, \tau_2,\, \tau_3)^T$, the derivative of ψ_{el} with respect to $\boldsymbol{\varepsilon}^e$ yields

$$\tilde{\boldsymbol{\tau}} = \mathbb{C}\,\boldsymbol{\varepsilon}^e \qquad \mathbb{C} = \kappa\,\mathbf{1} \otimes \mathbf{1} + 2\,\mu\,\mathbb{P} \tag{27}$$

with the bulk modulus $\kappa = \lambda + \frac{2}{3}\mu$ and the shear modulus $\mu = G$. The vector $\mathbf{1}$ is defined by $\mathbf{1} = (1,\, 1,\, 1)^T$ and the projection matrix $\mathbb{P}$ is given with $\mathbb{P} = \mathbb{I} - \frac{1}{3}\mathbf{1}\mathbf{1}^T$ where $\mathbb{I} = \mathrm{diag}(1,\, 1,\, 1)$.

Applying the logarithm function to $(24)_2$ yields an additive decomposition as follows

$$\boldsymbol{\varepsilon}^e_{trial} = \boldsymbol{\varepsilon}^e_{n+1} + \gamma_{n+1}\frac{\partial \phi_{n+1}}{\partial \tilde{\boldsymbol{\tau}}_{\,n+1}} \quad . \tag{28}$$

where $\boldsymbol{\varepsilon}^e_{trial} = (\varepsilon^e_1,\, \varepsilon^e_2,\, \varepsilon^e_3)^T_{trial}$ and $\varepsilon^e_{A_{trial}} = \log \lambda^e_{A_{trial}}$.

The yield condition is assumed to be of von Mises–type and can be written in terms of the eigenvalues of the Kirchhoff stress tensor. With a saturation–type function for isotropic hardening

it holds

$$\begin{aligned}\phi(\tilde{\boldsymbol{\tau}},\zeta) &= g-(y_0-\zeta)\\ g &= \sqrt{\tfrac{3}{2}\,\tilde{\boldsymbol{\tau}}^T\,\mathbb{P}\,\tilde{\boldsymbol{\tau}}}\\ -\zeta &= h\,\bar{\varepsilon}+(y_\infty-y_0)(1-\exp[-\eta\,\bar{\varepsilon}])\,,\end{aligned} \tag{29}$$

where, h, y_0, y_∞, η are material parameters. The derivative of the yield condition with respect to $\tilde{\boldsymbol{\tau}}$ and q is expressed as

$$\frac{\partial\phi}{\partial\tilde{\boldsymbol{\tau}}}=\frac{3}{2g}\,\mathbb{P}\,\tilde{\boldsymbol{\tau}} \qquad\qquad \frac{\partial\phi}{\partial\zeta}=1\,. \tag{30}$$

Hence, combining (27), (28) with (30) yields after some algebra

$$\tilde{\boldsymbol{\tau}}_{n+1}=\mathbb{C}\,\boldsymbol{\varepsilon}^e_{n+1}=(\mathbb{C}^{-1}+\frac{3\gamma_{n+1}}{2g_{n+1}}\mathbb{P})^{-1}\boldsymbol{\varepsilon}^e_{trial}\,. \tag{31}$$

As can be seen, the combination of the exponential mapping with the logarithmic strains leads to a stress projection algorithm in the space of principal stresses, which is identical to the infinitesimal theory, see also [20]. The unknown consistency parameter γ_{n+1} is iteratively determined by fulfillment of the yield condition (29) using a Newton iteration scheme. For the special case of linear hardening a direct solution of the yield criterion with respect to γ_{n+1} without iteration is possible.

The algorithmic elastoplastic tangent modul is derived as follows

$$\frac{\mathrm{d}\tilde{\boldsymbol{\tau}}_{n+1}}{\mathrm{d}\boldsymbol{\varepsilon}_{n+1}}=\kappa\,\mathbf{1}\otimes\mathbf{1}+2\mu\,\vartheta_1\,\mathbb{P}-2\mu\,\vartheta_2\,\mathbf{n}\otimes\mathbf{n}\,, \tag{32}$$

with

$$\begin{aligned}\mathbf{n} &= \frac{\operatorname{dev}\tilde{\boldsymbol{\tau}}_{trial}}{|\operatorname{dev}\tilde{\boldsymbol{\tau}}_{trial}|}\\ \vartheta_1 &= 1-\frac{3\,\mu\gamma_{n+1}}{g_{trial}}\\ \vartheta_2 &= \frac{3\,\mu}{3\,\mu+y'}+\frac{g_{n+1}}{g_{trial}}-1\\ y' &= h+(y_\infty-y_0)\,\eta\,\exp[-\eta\bar{\varepsilon}_{n+1}]\,.\end{aligned} \tag{33}$$

The function g_{trial} is defined with $(29)_2$ replacing $\tilde{\boldsymbol{\tau}}$ with $\tilde{\boldsymbol{\tau}}_{trial}=\mathbb{C}\,\boldsymbol{\varepsilon}^e_{trial}$.

Pullback of the Kirchhoff stress tensor yields the Second Piola Kirchhoff stress tensor $\mathbf{S}=\mathbf{F}^{-1}\boldsymbol{\tau}\mathbf{F}^{T-1}$ with eigenvalues $S_A=\frac{\tau_{A_{n+1}}}{\lambda^{e\ A}_{A_{trial}}}$.

The associated fourth order tangent tensor has been derived in [23]

$$\begin{aligned}\mathbb{C}_{ep}=&\textstyle\sum_{A=1}^{3}\sum_{B=1}^{3}C_{AABB}\,(\hat{\mathbf{N}}^A_{trial}\otimes\hat{\mathbf{N}}^A_{trial}\otimes\hat{\mathbf{N}}^B_{trial}\otimes\hat{\mathbf{N}}^B_{trial})\\ &+\textstyle\sum_{A\neq B}^{3}C_{ABAB}\,(\hat{\mathbf{N}}^A_{trial}\otimes\hat{\mathbf{N}}^B_{trial}\otimes\hat{\mathbf{N}}^A_{trial}\otimes\hat{\mathbf{N}}^B_{trial}\\ &\qquad+\hat{\mathbf{N}}^A_{trial}\otimes\hat{\mathbf{N}}^B_{trial}\otimes\hat{\mathbf{N}}^B_{trial}\otimes\hat{\mathbf{N}}^A_{trial})\end{aligned} \tag{34}$$

with the coefficients

$$C_{AABB} = \frac{\partial S_A}{\partial E_B} = \lambda^{e\,-2}_{A_{trial}} \left(\frac{\partial \tau_{A_{n+1}}}{\partial \varepsilon_{B_{n+1}}} - 2\,\tau_{A_{n+1}}\,\delta_{AB}\right) \lambda^{e\,-2}_{B_{trial}}$$
$$C_{ABAB} = \frac{1}{2}\,\frac{S_A - S_B}{E_A - E_B} = \frac{S_A - S_B}{\lambda^{e\,2}_{A_{trial}} - \lambda^{e\,2}_{B_{trial}}}\,. \tag{35}$$

As can be seen eq. (34) leads to symmetric tangent matrices.

5 Numerical examples

With the following five examples we demonstrate the behaviour of the developed hexahedral finite element in several nonlinear applications. Different modifications of elements based on the enhanced assumed strain method (EAS) and the assumed natural strain method (ANS) have to be distinguished. The introduced abbreviations to describe the special element types are given in Table 1. As an example, the element type Q1A2E5 denotes a standard displacement element(Q1) with assumed shear strain interpolation(A2) and five enhanced strain parameters(E5). In addition a Q1E30–element has been used for comparisons. This element is formulated with respect to a global Cartesian basis system and possesses 30 enhanced parameters for all strain components, see [14].

Abbr.	Description
Q1	Displacement based hexahedral element
A1	ANS on E_{33}
A2	ANS on E_{13} and E_{23}
A3	ANS on E_{13}, E_{23} and E_{33}
E5, E8	EAS with 5 or 8 parameters
E30	EAS with 30 parameters

Table 1
Abbreviations to denote different element types

5.1 Clamped cylindrical shell segment

In the first example we discuss the behaviour of a clamped cylindrical shell segment subjected to a single load $F = \lambda F_0$ with $F_0 = 200$ at the free end, see Figure 1. The geometrical data are: length of the cylinder $L = 304.8$, inner radius $R_i = 100.1$ and thickness $t = 3.0$. A corresponding example with isotropic material has been investigated e.g. in [24]. Here, we consider a composite material with the layer sequences $0°/90°/0°$ and $90°/0°/90°$, where $0°$ and $90°$ are related to the axial and circumferential direction of the cylinder. The data for the transversal isotropic material are given in Figure 1. Due to symmetry, only half of the system is discretized. The numerical calculations are performed with a regular and a distorted $16 \times 16 \times 1$ finite element mesh, see Figure 1.

Different aspects are discussed in the following. At first we compare our results for the hexahedral element Q1A3E5 to earlier calculations using a four–node shell element [25]. In Figure 2

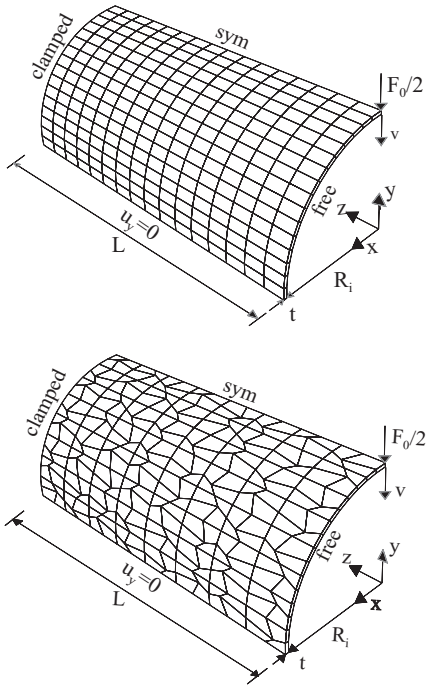

$$
\begin{aligned}
E_1 &= 2068.5 \\
E_2 &= 517.125 = E_3 \\
G_{12} &= 795.6 \quad = G_{13} = G_{23} \\
\nu_{12} &= 0.3 \quad = \nu_{13} = \nu_{23}
\end{aligned}
$$

Fig. 1. Cylindrical shell segment: regular and distorted FE–mesh

load deflection curves are depicted for both layer sequences. There is good agreement over the entire range of deformation for both elements. Next we investigate the influence of the ANS

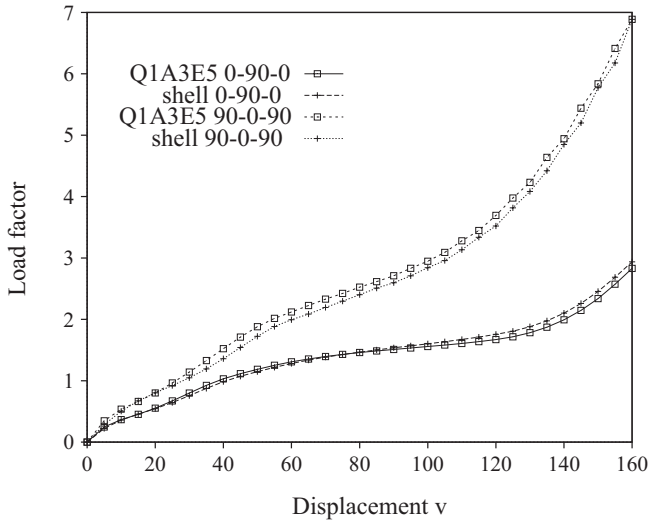

Fig. 2. Cylindrical shell segment: hexahedral versus shell–element

and EAS interpolations.In Figure 3 load deflection curves are depicted for different element types. Here, a layer sequence $90°/0°/90°$ has been used. According to Figure 2, results obtained with the Q1A3E5 element can be regarded as reference solution. It can be seen clearly that the Q1A1E5 element without ANS interpolation for the transverse shear strains is too stiff, even in the linear range. The next element, the Q1A3 element without enhanced strain formulation leads to correct deflections within the linear theory. However, with increasing load a locking effect can be observed. Nearly accurate results are obtained using the Q1A2E5 element. The additional ANS interpolation for the thickness strains in the Q1A3E5 element yields an improvement in the range of large deformations. This example shows that the EAS method applied to the membrane strains and thickness strains is less important than the ANS interpolation for the shear strains and thickness strains.

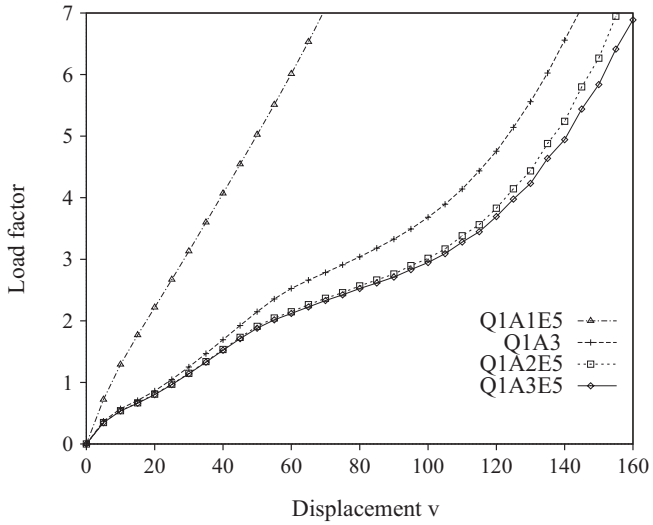

Fig. 3. Cylindrical shell segment: influence of ANS and EAS terms on hexahedral element

Finally we consider the influence of mesh distortion on the results. The used meshes are shown in Figure 1. Again a layer sequence 90°/0°/90° has been used. Here, we compare the Q1E30

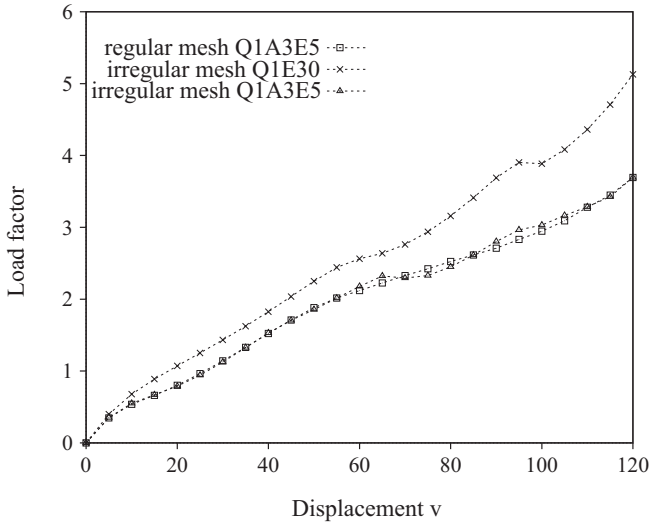

Fig. 4. Cylindrical shell segment: influence of mesh distortion

element with 30 enhanced assumed strain parameters with the Q1A3E5 element. As can be seen in Figure 4, the Q1A3E5 element is fairly insensitive with respect to mesh distortions. The Q1E30 element gives accurate results for the regular mesh but leads to considerable locking for the distorted mesh.

5.2 Slit tubular segment

In [26] Galletly and Guest have discussed the behaviour of a deployable structure, of tubular cross–section, manufactured from a novel composite layup. The stability behaviour has been investigated using a beam–type model. Here, we discretize the structure using the developed hexahedral elements. For simplicity we consider isotropic material behaviour. Geometrical and material data as well as loading and boundary conditions are depicted in Figure 5. Note that at $z = 0$ the tube is supported in z-direction, to avoid rigid body motions. The tube is loaded by a single moment at $z = L$. Four rigid body elements, described in [27], have been added to

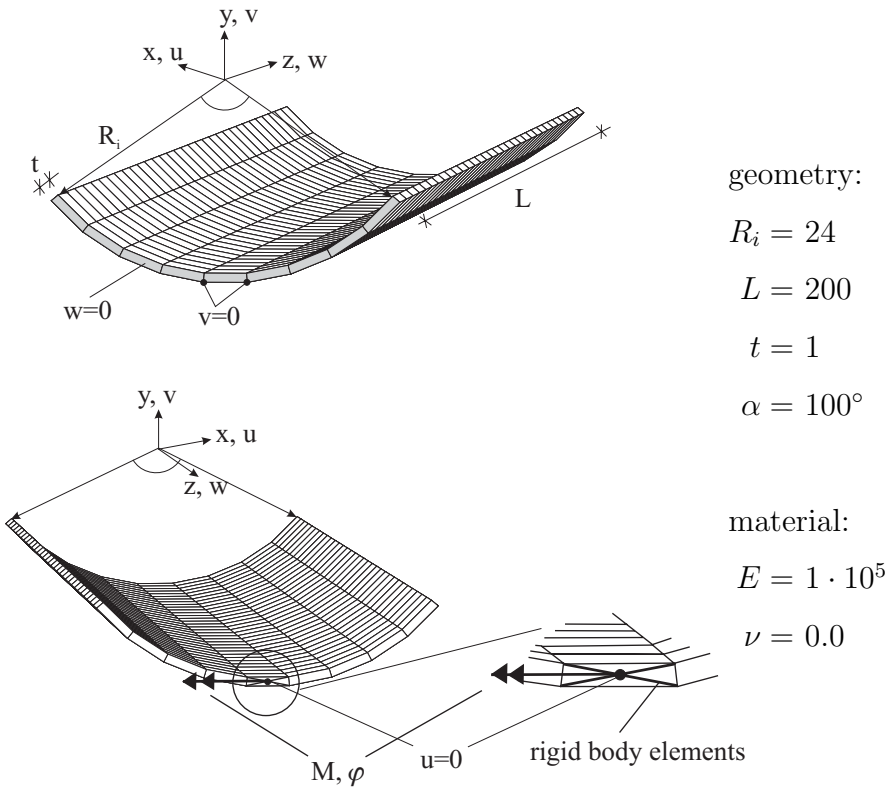

geometry:

$R_i = 24$

$L = 200$

$t = 1$

$\alpha = 100°$

material:

$E = 1 \cdot 10^5$

$\nu = 0.0$

Fig. 5. Tubular segment: geometry and material data

apply the loading on the hexahedral element. The structure is discretized with a $9 \times 32 \times 1$ mesh of Q1A3E5 elements.

A displacement driven calculation yields the load deflection curve depicted in Figure 6 for the moment $M = M_x$ versus the rotational degree of freedom $\varphi = \varphi_x$. A comparison with

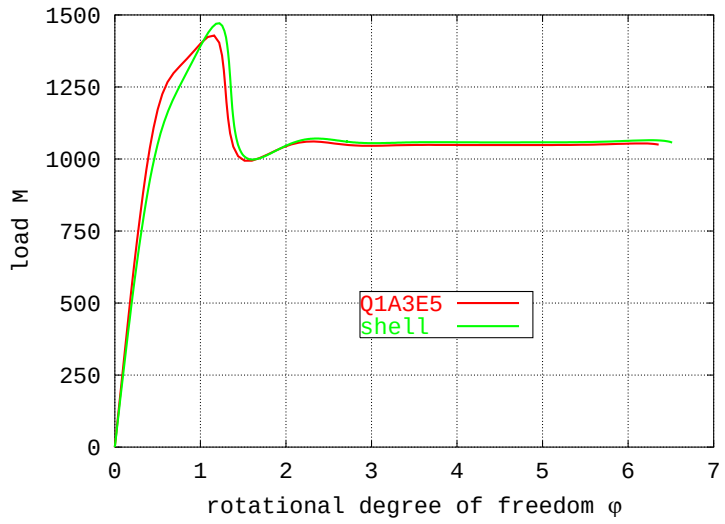

Fig. 6. Tubular segment: moment M versus rotational degree of freedom φ

results using again a four–node shell element [25] shows good agreement over the entire range of deformation.

The deformation behaviour of the tube is illustrated by different deformed meshes, see Figure 7. At $\varphi = 1.30$ a first limit point occurs. Here the initial curvature in transverse direction vanishes

at the loaded end. For rotational parameters $\varphi \geq 1.62$ the deformation takes place at a nearly constant moment.

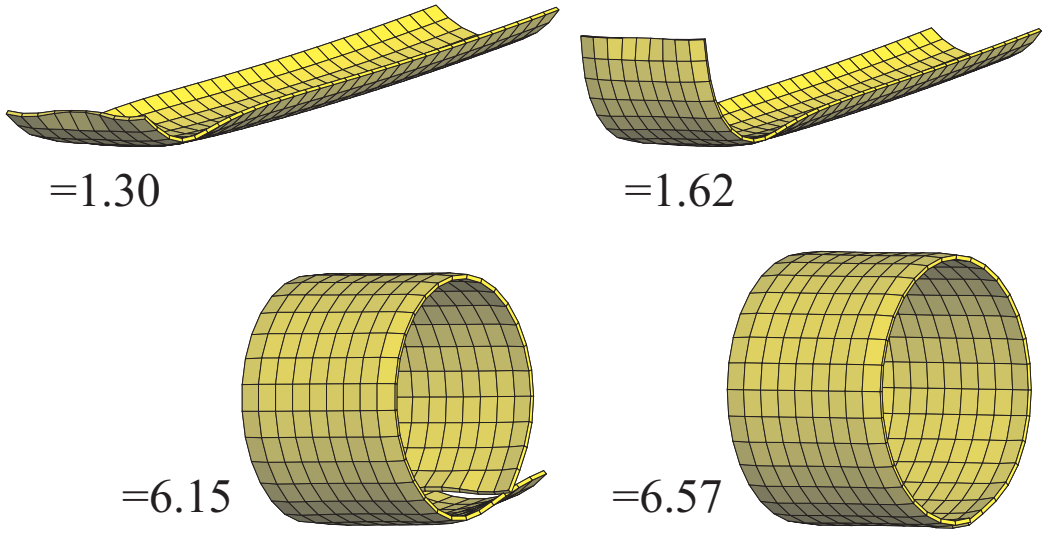

Fig. 7. Tubular segment: deformed systems at different load steps

5.3 *Pinched cylinder*

The pinched cylinder according to Figure 8 is a representative example for finite deformations. The cylinder is supported at one end by a rigid diaphragm. At the other end two opposite single loads act. The boundary conditions of the rigid diaphragm are modelled in two alternative ways. Model A approximates a soft support within a shell formulation, whereas model B provides an approximation for hard support.

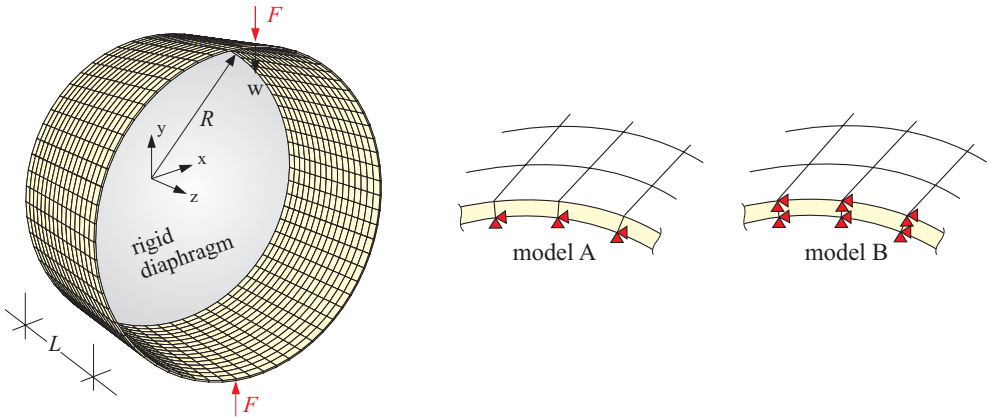

Fig. 8. Pinched cylinder: problem and modeling of boundary conditions at the rigid diaphragm

The geometry is described by: radius $R = 300$, length $L = 600$ and thickness $t = 3$. Furthermore, the material data are given for isotropic elastoplasticity: $E = 3000$, $\nu = 0.3$, $y_0 = 24.3$ and $h = 300$. Considering symmetry, only one quarter of the cylinder is discretized with 16x16x1 elements. The computed load deflection curves are depicted in Figure 9. As can be seen there is good agreement for model B with a reference solution [4], whereas the boundary conditions of model A lead to a different results. A deformed configuration at $w = 250$ and the equivalent

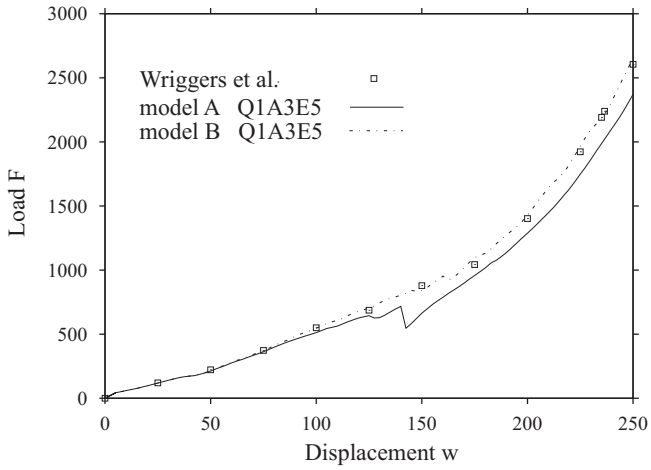

Fig. 9. Pinched cylinder: load deflection curves for different boundary conditions

plastic strains are depicted in Figure 10.

5.4 *Conical shell*

With this example we investigate the elastoplastic behaviour of a conical shell under ring load. The geometrical data are taken from Başar and Itskov [28], who investigated this problem

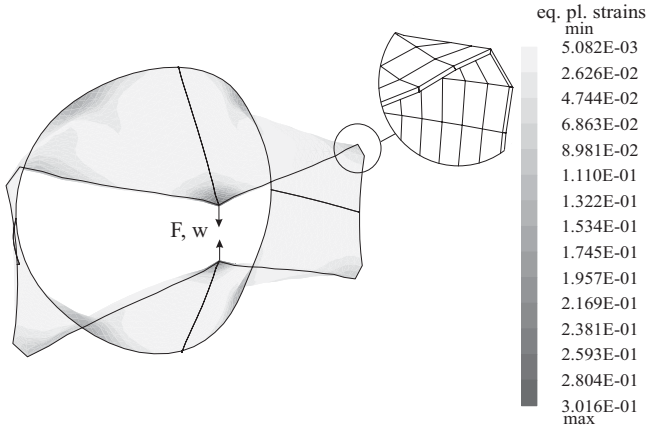

Fig. 10. Pinched cylinder: deformed mesh and distribution of equivalent plastic strains at w=250

in case of an Ogden material. All necessary data are depicted in Figure 11. The system is slightly modified due to eccentric loading and boundary conditions. Considering symmetry,

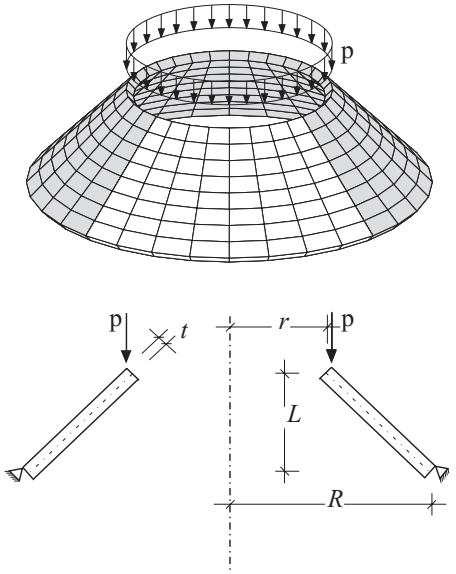

geometry:	material:
$r = 1$	$E = 206.9$
$R = 2$	$\nu = 0.29$
$L = 1$	$y_0 = 0.45$
$t = 0.1$	$y_\infty = 0.715$
load:	$h = 0.12924$
$p = 1$	$\eta = 16.93$

Fig. 11. Conical shell: finite element mesh with geometry and material data

only a quarter of the conical shell is discretized with 8x8x1 Q1A3E5 elements. Thus only symmetric buckling behaviour may occur. For this problem a nine point integration scheme has been introduced to avoid zero energy modes, see [29]. The nonlinear behaviour is computed using an arc–length algorithm with displacement control. The results are depicted in Figure 12, where w denotes the vertical displacement of the upper outside edge. The load is increased until $w = 0.02$, where the elastic limit is reached. Hence a rolling process starts at top of the conical shell. A further stability point is traced at $w = 1.21$. Here, a global snap through behaviour of the shell is observed. This is also shown with the deformed meshes in Figure 13. A local minimum of the load deflection curve is attained at $w = 1.75$. Then a stable path with increasing loads due to stiffening effects arises. The structure is unloaded at a total deflection of $w = 2.25$. Figure 12 shows the completely unloaded shell at $w = 2.239$. Finally the initial mesh and the final deformed mesh of the unloaded shell are plotted in Figure 14. As can be seen there is relatively little elastic spring back.

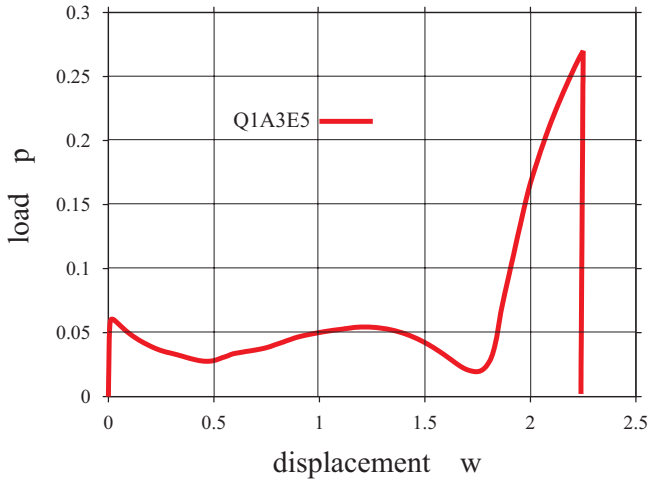

Fig. 12. Conical shell: ring load p versus vertical displacement w of the upper edge

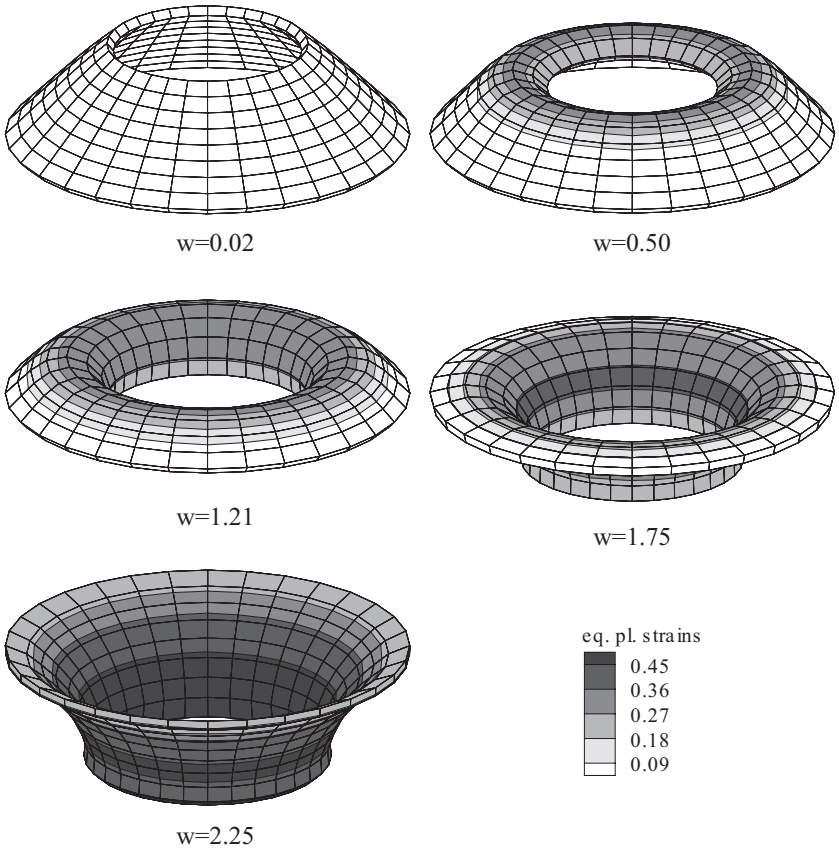

Fig. 13. Conical shell: deformed meshes and associated equivalent plastic strains

5.5 Hemispherical shell

This example provides a standard test in linear and nonlinear shell computations. A hemispherical shell with an 18° hole is loaded by four opposite forces. The material and geometry data are given in Figure 15. Considering symmetry, only a quarter of the shell is discretized with 16x16x1 Q1A3E5 elements. The details of the loading are depicted in Figure 15. Here we investigate the element behaviour within a dynamic problem. Applying a pulse loading according to Figure 16, the answer of the system is evaluated using a standard Newmark algorithm. We choose a constant time step $\Delta t = 10^{-5}$. Results for the displacements u_A and u_B are presented in Figure 17, whereas deformed meshes are depicted in Figure 18.

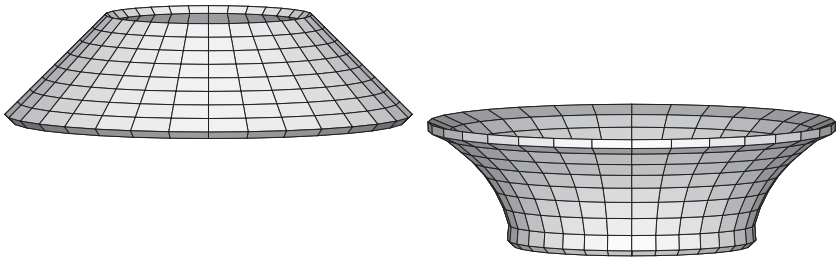

Fig. 14. Conical shell: initial and deformed unloaded system

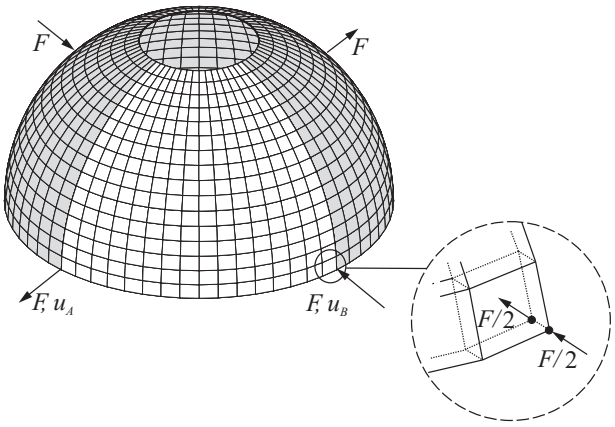

geometry:

$R = 10$

$t = 0.01$

material:

$E = 6.825 \cdot 10^7$

$\nu = 0.3$

$\rho = 2.0 \cdot 10^{-}6$

Fig. 15. Hemispherical shell: geometry and material data

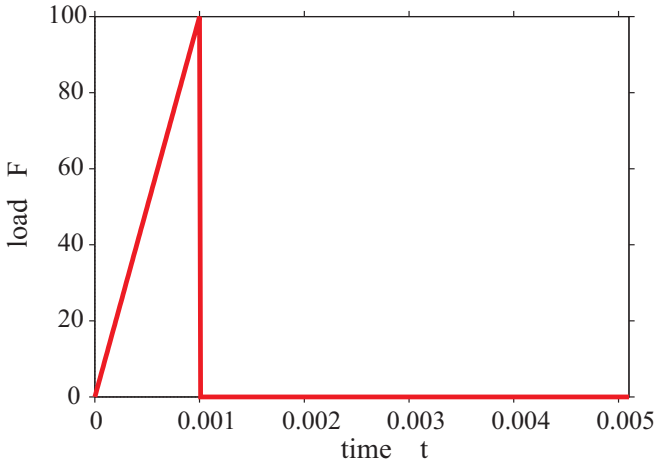

Fig. 16. Hemispherical shell: load time history

6 Conclusions

In this paper a continuum based hexahedral shell element has been presented. Assumed natural strain method and enhanced assumed strain method have been used to improve the relative poor element behaviour of the displacement element. Numerical tests have shown that the ANS–interpolations for the transverse shear strains and the thickness strains are essential for a locking–free element behaviour. Due to the developed techniques an element orientation exists which has to be taken into account within the mesh generation. For the EAS–interpolations it turns out that many enhanced parameters lead to a loss of robustness within the equilibrium iteration. This holds especially for inelastic computations. Furthermore, only minor improvements can be achieved with more than five parameters. Based on the described numerical tests

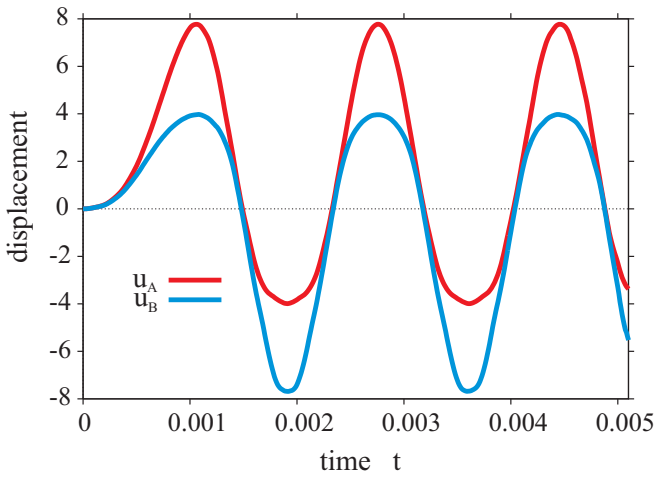

Fig. 17. Hemispherical shell: displacements u_A and u_B versus time

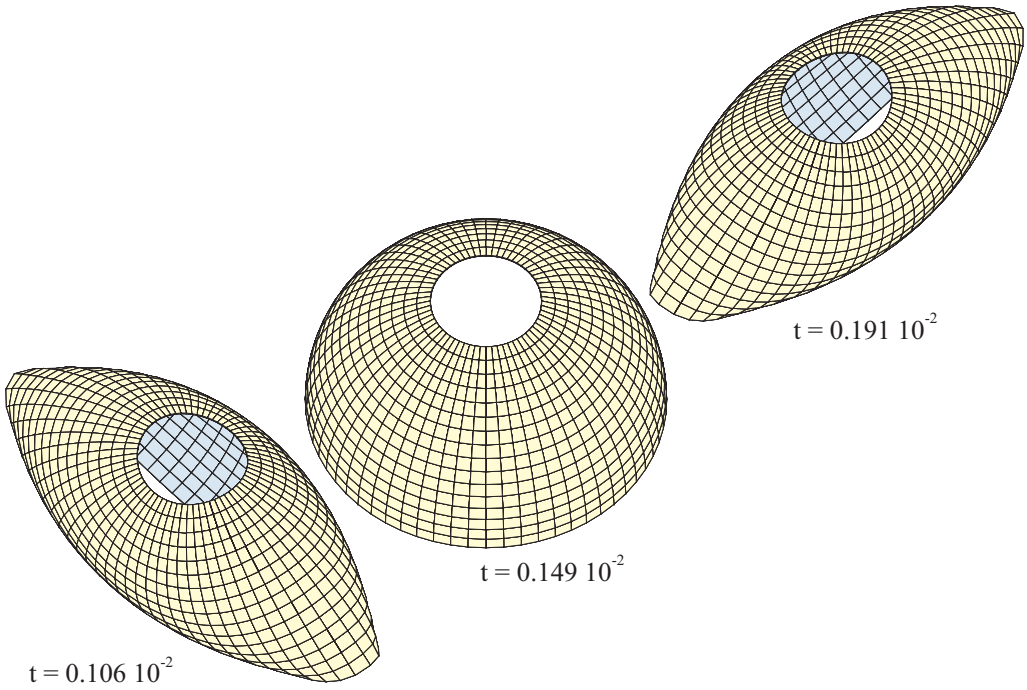

Fig. 18. Hemispherical shell: deformed configurations

the Q1A3E5–element is recommended for the nonlinear analysis of thin–walled shell structures. The presented examples show the range of applicability and the efficiency of the developed element formulation.

References

[1] Krätzig WB. 'Best' transverse shearing and stretching shell theory for nonlinear finite element simulations. Computer Methods in Applied Mechanics and Engineering 1993; 103:135–160.

[2] Büchter N, Ramm E, Roehl D. Three–dimensional extension of nonlinear shell formulation based on the enhanced assumed strain concept. International Journal for Numerical Methods in Engineering 1994; 37: 2551–2568.

[3] Betsch P, Stein E. An assumed strain approach avoiding artificial thickness straining for a nonlinear 4–node shell element. Communications in Numerical Methods in Engineering 1995;

11:899–909.

[4] Wriggers P, Eberlein R, Reese S. A comparison of three–dimensional continuum and shell elements for finite plasticity. International Journal of Solids and Structures 1996; 33:3309–3326.

[5] Simo JC, Rifai MS. A class of mixed assumed strain methods and the method of incompatible modes. International Journal for Numerical Methods in Engineering, 1990; 29:1595–1638.

[6] Simo JC, Armero F. Geometrically non-linear enhanced strain mixed methods and the method of incompatible modes. International Journal for Numerical Methods in Engineering 1992; 33:1413–1449.

[7] Parisch H. A continuum-based shell theory for non-linear applications. International Journal for Numerical Methods in Engineering 1995; 38:1855–1883.

[8] Miehe C. A theoretical and computational model for isotropic elastoplastic stress analysis in shells at large strains. Computer Methods in Applied Mechanics and Engineering 1998; 155:193–223.

[9] Hauptmann R, Schweizerhof K. A systematic development of 'solid–shell' element formulations for linear and non–linear analyses employing only displacement degrees of freedom. International Journal for Numerical Methods in Engineering, 1998; 42:49–69.

[10] Klinkel S, Gruttmann F, Wagner W. A continuum based 3d–shell element for laminated structures. Computers & Structures 1999; 71:43–62.

[11] Bathe KJ, Dvorkin EN. A continuum mechanics based four node shell element for general nonlinear analysis. Engineering Computations 1984; 1:77–88.

[12] Ibrahimbegović A. Finite elastoplastic deformations of space-curved membranes. Computer Methods in Applied Mechanics and Engineering 1994; 119:371–394.

[13] Betsch P, Gruttmann F, Stein E. A 4–node finite shell element for the implementation of general hyperelastic 3d–elasticity at finite strains. Computer Methods in Applied Mechanics and Engineering 1996; 130:57–79.

[14] Klinkel S, Wagner W. A geometrical non-linear brick element based on the eas–method. International Journal for Numerical Methods in Engineering 1997; 40:4529–4545.

[15] Ramm E, Bischoff M, Braun M. Higher order nonlinear shell formulations – a step back into three dimensions. In Trondheim K. Bell (Ed.) Dept. of Structural Engineering Norwegian Institute of Technology, From Finite Elements to the Troll Platform, Norway 1994; 65–88.

[16] Betsch P. Statische und dynamische Berechnungen von Schalen endlicher elastischer Deformationen mit gemischten finiten Elementen. Forschungs- und Seminarberichte aus dem Bereich der Mechanik der Universität Hannover, Bericht F 96-4 1996.

[17] Spencer AJM. Continuum models of fibre-reinforced materials. In A.P.S. Selvadurai, editor, Mechanics of Structured Media, Proceedings of the International Symposium on the Mechanical Behavior of Structured Media, Ottawa, Amsterdam/Oxford/New York, Elsevier Scientific Publishing Company 1981: 3–18.

[18] Boehler JP. Introduction to the invariant formulation of anisotropic constitutive equations. In J.P. Boehler, editor, Application of Tensor Functions in Solid Mechanics, CISM Courses and Lectures No. 292, Wien/New York, Springer-Verlag; 1987: 13–64.

[19] Miehe C, Stein E. A canonical model of multiplicative elasto-plasticity formulation and aspects of the numerical implementation. European Journal of Mechanics A 1992; 11:25–43.

[20] Simo JC. Algorithms for static and dynamic multiplicative plasticity that preserve the classical return mapping schemes of the infinitesimal theory. Computer Methods in Applied Mechanics and Engineering 1992; 99:61–112.

[21] Weber G, Anand L. Finite deformation constitutive equations and a time integration procedure for isotropic, hyperelastic–viscoelastic solids. Computer Methods in Applied Mechanics and Engineering 1990; 79:173–202.

[22] Betsch P, Stein E. Numerical implementation of multiplicative elasto-plasticity into assumed strain elements with application to shells at large strains. Computer Methods in Applied Mechanics and Engineering 1999; 179:215-245.

[23] Chadwick P, Ogden RW. On the definition of elastic material. Archive for Rational Mechanics and Analysis, 1971; 44:41–53.

[24] Stander N, Matzenmiller A, Ramm E. An assessment of assumed strain methods in finite rotation shell analysis. Engineering Computations 1989; 6:58–66.

[25] Wagner W, Gruttmann F. A simple finite rotation formulation for composite shell elements. Engineering Computations 1994; 11:145–176.

[26] Galletly DA, Guest SD. Equilibrium and stability analysis of composite slit tubes. in: Proceedings of the IASS-IACM 2000, Fourth International Colloquium on Computation of Shell & Structures. IASS-IACM, 2000.

[27] Wagner W, Gruttmann F. Modeling of Shell–Beam Transitions in the Presence of Finite Rotations, Computer Assisted Mechanics and Engineering Sciences, accepted for publication, 2001.

[28] Başar Y, Itskov M. Finite element formulation of the Ogden material model with application to rubber-like shells. International Journal for Numerical Methods in Engineering 1998; 42:1279–1305.

[29] Simo JC, Armero F, Taylor RL. Improved version of assumed enhanced strain tri–linear elements for 3d finite deformation problems. Computer Methods in Applied Mechanics and Engineering 1993; 110:359–386.